Postnatal Ablation of POMC Neurons Induces an Obese Phenotype Characterized by Decreased Food Intake and Enhanced Anxiety-Like Behavior

Yona Greenman,* Yael Kuperman,* Yonat Drori, Sylvia L. Asa, Inbal Navon, Oren Forkosh, Shosh Gil, Naftali Stern, and Alon Chen

Institute of Endocrinology, Metabolism, and Hypertension (Y.G., N.S.), Tel Aviv-Sourasky Medical Center and Sackler School of Medicine, Tel Aviv University, Tel Aviv 69978, Israel; Departments of Veterinary Resources (Y.K.) and Neurobiology (Y.G., Y.K., Y.D., I.N., O.F., S.G., A.C.), Weizmann Institute of Science, Rehovot 76100, Israel; and Department of Laboratory Medicine and Pathobiology (S.L.A.), University of Toronto, Toronto, Canada M5G 2C4

Proopiomelanocortin (POMC) neurons in the arcuate nucleus of the hypothalamus are central components of systems regulating appetite and energy homeostasis. Here we report on the establishment of a mouse model in which the ribonuclease III ribonuclease Dicer-1 has been specifically deleted from POMC-expressing neurons ($POMC^{\Delta DCR}$), leading to postnatal cell death. Mice are born phenotypically normal, at the expected genetic ratio and with normal hypothalamic POMC-mRNA levels. At 6 weeks of age, no POMC neurons/cells could be detected either in the arcuate nucleus or in the pituitary of $POMC^{\Delta DCR}$ mice. $POMC^{\Delta DCR}$ develop progressive obesity secondary to decreased energy expenditure but unrelated to food intake, which was surprisingly lower than in control mice. Reduced expression of AgRP and ghrelin receptor in the hypothalamus and reduced uncoupling protein 1 expression in brown adipose tissue can potentially explain the decreased food intake and decreased heat production, respectively, in these mice. Fasting glucose levels were dramatically elevated in $POMC^{\Delta DCR}$ mice and the glucose tolerance test revealed marked glucose intolerance in these mice. Secondary to corticotrope ablation, basal and stress-induced corticosterone levels were undetectable in $POMC^{\Delta DCR}$ mice. Despite this lack of activation of the neuroendocrine stress response, $POMC^{\Delta DCR}$ mice exhibited an anxiogenic phenotype, which was accompanied with elevated levels of hypothalamic corticotropin-releasing factor and arginine-vasopressin transcripts. In conclusion, postnatal ablation of POMC neurons leads to enhanced anxiety and the development of obesity despite decreased food intake and glucocorticoid deficiency. **(*Molecular Endocrinology* 27: 1091–1102, 2013)**

The long-term maintenance of stable body weight and energy homeostasis depends on the interplay between several central and peripheral systems. Broadening our understanding of the regulation of these processes is critical for developing tools to cope with the ever-expanding prevalence of obesity, with its associated morbidity and mortality (1). The hypothalamus is the key brain region that integrates peripheral signals relaying information on the nutritional state and the changing energy requirements (2).

Two neuronal populations situated in the arcuate nucleus of the hypothalamus are central to the integration and processing of information related to energy homeostasis as well as to the translation of this information into

ISSN Print 0888-8809 ISSN Online 1944-9917
Printed in U.S.A.

Received October 24, 2012. Accepted May 9, 2013.
First Published Online May 15, 2013

* Y.G. and Y.K. contributed equally to this study.

Abbreviations: Adrb3, β-3 adrenergic receptor; AgRP, agouti-related protein; ASR, acoustic startle response; AVP, arginine-vasopressin; BAT, brown adipose tissue; CRF, corticotropin-releasing factor; CRFR1, CRF receptor 1; DIO2, type II iodothyronine deiodinase; GHSR, ghrelin receptor; GLP-1, glucagon-like peptide 1; H&E, hematoxylin and eosin; HOMA-IR, homeostasis model assessment insulin resistance index; HPA, hypothalamus-pituitary-adrenal; NPY, neuropeptide Y; NTS, nucleus of the solitary tract; PND, postnatal day; POMC, proopiomelanocortin; PVN, paraventricular nucleus; UCP1, uncoupling protein 1; YFP, yellow fluorescent protein.

signals impacting on appetite and energy expenditure. The first is the neuropeptide Y (NPY) and agouti-related protein (AgRP) containing neurons that are stimulated by ghrelin and inhibited by leptin with the net effect of increasing appetite (3); and second are the proopiomelanocortin (POMC)- and cocaine and amphetamine-regulated transcript-containing neurons that are stimulated by leptin. POMC is processed to α-MSH that acts on melanocortin receptor 4 (MC4R) expressed in neurons situated in the hypothalamic paraventricular nucleus (PVN) and the nucleus of the solitary tract (NTS) in the hindbrain, thus suppressing appetite and increasing energy expenditure (4). NPY/AgRP neurons may reduce the melanocortinergic tone by activation of Y1 receptors on POMC neurons, and/or by direct AgRP antagonism of MC4R-expressing PVN neurons (2).

The clinical importance of the melanocortin system in weight regulation is evident from patients harboring mutations in the *pomc* gene (5), in the prohormone convertase 1 (6), and in the *mc4r* gene (7). These monogenic forms of obesity are characterized by early-onset hyperphagia and an extreme obese phenotype. Similar phenotypes also occur in POMC knockout mice models (8, 9). Although slightly different strategies were used to generate these POMC-deficient mice, the end point was similar, ie, a complete ablation of POMC-derived peptides. Despite that, it was striking to find significant phenotype differences between these models, mainly related to the onset of obesity, thyroid function, and glucose levels. The possible impact of compensatory changes on normal physiology and on our ability to interpret the resulting phenotypic changes is a well-recognized limitation of developmental models of genetic manipulations (10). Furthermore, knowledge obtained from isolated knockout of the *pomc* gene may not fully reveal the whole span of functions mediated by the POMC neuron.

To better characterize the physiological roles of the POMC neuron, we sought to establish a mouse model in which ablation of POMC-expressing neurons is achieved early in the postnatal period. To this end, we chose to genetically delete the ribonuclease III ribonuclease Dicer-1 (*dcr-1*) gene specifically from POMC neurons ($POMC^{\Delta DCR}$ mice), based on the knowledge that Dicer ablation has been shown to deplete cells of mature microRNAs, leading to apoptosis and cell death (11). Using this model, we show that postnatal ablation of POMC neurons leads to the development of obesity, insulin resistance, and enhanced anxiety-like behavior despite decreased food intake and glucocorticoid deficiency.

Materials and Methods

Animals

Mice were maintained in a pathogen-free, temperature-controlled (22°C ± 1°C) mouse facility on a reverse 12-hour light, 12-hour dark cycle at the Weizmann Institute of Science, according to institutional guidelines. Food and water were given ad libitum. Mice were fed regular chow diet (Harlan Biotech Israel Ltd, Rehovot, Israel). All experimental protocols were approved by the Institutional Animal Care and Use Committee of the Weizmann Institute of Science.

For the experiments described here, *Pomc*-Cre mice (stock number 005965; Jackson Laboratory, Bar Harbor, Maine) were initially mated with mice carrying the Dicer-1^{flox} allele (12). Hemizygous *Pomc*-Cre and heterozygous $Dicer1^{flox}$ offspring were then intercrossed to produce study animals. For visualizing POMC neurons, mice were crossed with the conditional R26R YFP reporter line (12). The *Pomc*-Cre mice were genotyped using the following primers: forward (TGCCACGACCAAGTGACAGC), reverse (CCAGGTTACGGATATAGTTCAT), with an annealing temperature of 55°C. The Dicer-1^{flox} mice were genotyped as previously described (13). The conditional R26R YFP reporter mice were genotyped using the following oligonucleotide primers: wild type (GCGAAGAGTTTGTCCTCAACC), transgene (AAAGTCGCTCTGAGTTGTTAT), and wild type reverse (GGAGCGGGAGAAATGGATATG), with an annealing temperature of 60°C.

Histological and immunohistological analysis

Mice were crossed with a Rosa26 YFP reporter mouse line for the detection of POMC neurons in the adult. Mice were transcardially perfused with 4% paraformaldehyde, and brains were sectioned on a freezing sliding microtome. Immunostaining for yellow fluorescent protein (YFP) was performed using biotinylated anti-green fluorescent protein antibody raised in goat as primary antibody (Abcam, Cambridge, United Kingdom). Streptavidin-conjugated Cy3 was used as secondary antibody (Jackson ImmunoResearch Laboratories Inc, West Grove, Pennsylvania). Fluorescence images were captured using a Nikon i80 microscope (Nikon, Tokyo, Japan).

For morphological studies, the pituitaries were sectioned horizontally and slides were stained with hematoxylin and eosin and with immunohistochemistry to localize ACTH as described previously (14). Immunolocalization was detected with the streptavidin-biotin-peroxidase complex technique and 3,3′-diaminobenzidine. Negative controls were performed with normal rabbit serum replacing the primary antiserum and after preabsorption of the primary antiserum with purified antigen.

Adrenal paraffin sections were stained by Mayer's hematoxylin and eosin (H&E) by a standard procedure.

Interscapular brown adipose tissue (BAT) was processed for immunohistochemical staining for Ucp1. Immunohistochemistry was carried out on paraffin sections with the avidin-biotin-peroxidase (avidin biotin complex method; Vector Laboratories, Burlingame, California) using the rabbit anti-Ucp1 Ab (Abcam). Sections were lightly counterstained with hematoxylin.

Circulating corticosterone levels

For the evaluation of the endocrine response to stress, tail blood samples were collected before (basal), immediately after 25 minutes of restraint stress, and 80 and 120 minutes after stress initiation. Restraint stress was induced using a 50-mL ventilated conical tube. Plasma samples were immediately centrifuged and stored at −80°C until assays for hormone measurement were conducted. Corticosterone concentrations were quantified using a corticosterone enzyme immunoassay kit (Cayman Chemical Co, Ann Harbor, Michigan).

Plasma hormones and lipid level measurement

After a 5-hour fasting period, mice were killed and trunk blood was collected. Plasma samples were immediately centrifuged and stored at −80°C. Free T_4 and TSH were measured by chemiluminescence (Advia Centaur; Siemens, Melvern, Pennsylvania). Cholesterol and triglycerides were measured in a chemical autoanalyzer (Advia 1650; Siemens, Melvern, Pennsylvania). The MILLIPLEX MAP mouse gut hormone panel (Millipore Corp, St Charles, Missouri) was used for the simultaneous quantification of active glucagon-like peptide 1 (GLP-1), insulin, and leptin in mouse plasma according to the manufacturer's protocol. Briefly, MILLIPLEX MAP is based on the Luminex xMAP technology, which uses internally color-coded microspheres with fluorescent dyes, thus creating distinctly colored bead sets, each of which is coated with a specific capture antibody. After an analyte from a test sample is captured by the bead, a biotinylated detection antibody is introduced, and the reaction mixture is then incubated with the streptavidin-phycoerythrin conjugate, the reporter molecule, to complete the reaction on the surface of each microsphere. The antibody pairs in the panel are specific to the desired analyte and exhibit no or negligible cross-reactivity with other analytes in the panel. Samples are read on a Luminex 200. The intraassay and interassay variations are less than 7% and less than 23%, respectively. Assay sensitivities [minimum detectable concentrations (picograms per milliliter)] for insulin, leptin, and GLP-1 are 25, 22, and 15 pg/mL, respectively.

Homeostasis model assessment insulin resistance index (HOMA-IR) calculation

The baseline degree of insulin resistance was estimated by homeostasis model assessment according to the method described by Matthews et al (15). In particular, an insulin resistance score (HOMA-IR) was computed with the formula: fasting plasma glucose (milligrams per deciliter) × fasting serum insulin (milliunits per liter)/405. Low HOMA-IR values indicate high insulin sensitivity, whereas high HOMA-IR values indicate low insulin sensitivity (insulin resistance).

Metabolic studies

Indirect calorimetry and food and water intake as well as locomotor activity were measured using the Labmaster system (TSE-Systems, Bad Homburg, Germany). The LabMaster instrument consists of a combination of feeding and drinking sensors for automated online measurement. The calorimetry system is an open-circuit system that determines O_2 consumption, CO_2 production, and respiratory exchange ratio. A photobeam-based activity monitoring system detects and records ambulatory movements, including rearing in every cage. All the parameters are measured continuously and simultaneously. Data were collected after 48 hours of adaptation in acclimated singly housed mice. Cumulative food intake data was recorded every 30 seconds and was further used for meal microstructure analysis.

Meal microstructure analysis

We used a 2-state hidden Markov model (16) to distinguish between a state of hunger and a state of satiation, which are characterized by a different distribution of food and water intake. These distributions were estimated from the eating and drinking patterns of 8 control mice during 1 day. In addition, these data were used to estimate the probabilities of transition between the states. These probabilities as well as the state distribution were estimated using the Baum-Welch algorithm (17). In the test, we found the most likely state sequence that matched the data. In this way we were able to identify epochs of eating out of hunger, which we dubbed as meals. The sequences were found using the Viterbi dynamic programming algorithm (18).

Glucose tolerance tests

Glucose tolerance tests were performed in awake animals during the dark phase of the day cycle. Following 6 hours of fasting, glucose (2 g/kg of body weight) was injected ip, and whole venous blood obtained from the tail vein at 0, 15, 30, 60, 90, and 120 minutes after the injection was measured for glucose using an automatic glucometer (Accu-Check performa; Roche Diagnostics GmbH, Mannheim, Germany).

Core body temperature

Core body temperature was measured using rectal thermometer at a constant hour during 3 consecutive days.

Body composition

Body composition was assessed using Echo-MRI (Echo Medical Systems, Houston, Texas).

Behavioral tests for anxiety-like behavior

All behavioral studies were performed during the dark phase after habituation to the test room for 2 hours before any test. For the assessment of anxiety-like behaviors, the light-dark transfer and the elevated plus maze tests were used. The set-up for the light-dark transfer test consists of 2 compartments, a dark one (14 × 27 × 26 cm) and a 950-lux illuminated lit compartment (30 × 27 × 26 cm), connected by a small passage. Mice were placed in the dark compartment to initiate a 5-minute test session. The time spent in the lit compartment, the number of entries to the lit compartment, and the latency of entering the lit zone were measured. The indices collected in these tests were quantified using an automated video tracking system (VideoMot2; TSE Systems).

The elevated plus maze apparatus is comprised of a central part (5 × 5 cm), 2 opposing open arms, and 2 opposing closed arms (30.5 × 5 × 15 cm). The apparatus was elevated to a height of 55 cm, and the open arms were illuminated with 6 lux. Mice were placed in the center, facing an open arm to initiate a 5-minute session test. The time spent in the open arms and the number of entries to the open arms was measured.

Acoustic startle response test

The acoustic startle response (ASR) test was performed as previously described (19). Briefly, the ASR session started with a 5-minute acclimatization period, with background white noise [70 dB(A)], which was maintained throughout the session. Overall, 32 startle stimuli [120 dB(A), 40 milliseconds; intertrial interval (randomly varying): 12–30 seconds] were presented; the stimulus presentations were divided into three blocks: blocks 1 and 3 each consisted of 6 startle stimuli, whereas block 2 consisted of 10 startle stimuli and 10 no stimuli [70 dB(A), 40 milliseconds; ie, equivalent to the background white noise] that were presented in a quasirandom manner. The entire ASR test session was completed in 20 minutes. Two indices were recorded: 1) mean maximal ASR (grams) (ie, the mean maximal ASR of the responses to the startle stimuli in block 2); and 2) the rate of habituation to the startle stimuli within a session [ie, the percentage change in mean maximal ASR (grams) of block 3 compared with that of block 1].

RNA preparation and real-time PCR

Total RNA was extracted from hypothalami, pituitaries, or BAT using a 5 Prime PerfectPure RNA cell and tissue kit (5 Prime GmbH, Hamburg, Germany). RNA was reverse transcribed to generate cDNA using high capacity cDNA reverse transcription kit (Applied Biosystems Inc, Foster City, California). The cDNA products were used as templates for real-time PCR analysis. Sense and antisense primers were selected to be located on different exons to avoid false-positive results caused by DNA contamination. Oligonucleotide primers for real-time PCR analysis of uncoupling protein 1 (UCP1) and peroxisome proliferator-activated receptor γ coactivator 1α were used as described (20). All other primers (Table 1) were designed using Primer Express software (Applied Biosystems, PerkinElmer, Foster City, California). Hypoxanthine guanine phosphoribosyl transferase 1 served as an internal control. Real-time PCRs were carried out on a 7500 real-time PCR system using fluorescent SYBR Green technology (Applied Biosystems). Reaction protocols had the following format: 10 minutes at 95°C for enzyme activation followed by 45 cycles of 15 seconds at 94°C and 60 seconds at 60°C. The specificity of the amplification products was checked by melting curve analysis.

Statistical analysis

Results are expressed as means ± SEM. Statistical analysis was performed using ANOVA or repeated-measurements 2-way ANOVA with post hoc Student's *t* tests or paired Student's *t* tests, as appropriate using JMP software (SAS Institute, Cary, North Carolina) (*, $P < .05$; **, $P < .01$).

Results

POMC$^{\Delta DCR}$ mice lose their POMC-expressing neurons and pituitary corticotropes

To establish a mouse line in which the POMC neurons are ablated postnatally, we cross-bred mice carrying conditional Dicer alleles (13), DCR$^{flox/flox}$, with mice expressing Cre recombinase specifically in POMC-expressing neurons/cells (21) (Figure 1A). The R26R-YFP conditional reporter alleles (12) in the genetic background of the DCR$^{flox/flox}$ mouse line enabled the detection of Cre-mediated recombination by the induction of YFP expression (Figure 1, A and B).

POMC$^{\Delta DCR}$ mice are born phenotypically normal and at the expected genetic ratio. In contrast with the strong YFP immunostaining obtained in control animals, no POMC neurons could be detected in the arcuate nucleus of the hypothalamus in POMC$^{\Delta DCR}$ mice at 6 weeks of age, indicating that microRNAs are essential for survival of these neurons (Figure 1B). Accordingly, POMC-mRNA expression in the hypothalamus of 2-month-old mice was reduced by 96% compared with control animals ($P < .001$, Figure 1C). To establish the time course of this neuronal loss, POMC-mRNA expression was examined in hypothalami excised at sequential time points. On postnatal day (PND) 1, POMC-mRNA expression is similar in POMC$^{\Delta DCR}$ and their control littermates, whereas at PND7 and PND21, there was a reduction of 35% and

Table 1. Primers Used for Real-Time PCR Analysis

Gene	Forward Primer	Reverse Primer	GenBank Accession Number
Adrb3	GGCAACCTGCTGGTAATCAT	GCATTACGAGGAGTCCCAC	NM_013462.3
AgRP	AAGCTTTGGCGGAGGTGCTAGAT	AAGCAGGACTCGTGCAGCCTTACA	NM_007427.2
AVP	TCAACACTACGCTCTCCGCTT	CCTTTGCCGCCCGG	NM_009732.1
CRFR1	TGCCAGGAGATTCTCAACGAA	AAAGCCGAGATGAGGTTCCAG	NM_007762.4
DIO2	TCCTCCTAGATGCCTACAAACAGG	ATTCAGGATTGGAGACGTGCAC	NM_010050.2
GHSR	AAACAGACAGTGAAGATGCTTGCTG	GGCTCGAAAGACTTGGAAAACAG	NM_177330.4
HPRT1	GCAGTACAGCCCCAAAATGG	GGTCCTTTTCACCAGCAAGCT	NM_013556
Leptin R	ACACTGAAGGGAAGACACTG	GGGTTCTTAGGTAATGGCTCC	NM_146146
MC3R	CTGTAGCAACGGGTGTCGG	ATCAGCCTGCCTCATCCC	NM_008561.3
MC4R	CAAGAACCTGCACTCACCCA	GACCCATTCGAAACGCTCAC	NM_016977.3
NPY	TCAGACCTCTTAATGAAGGAAAGCA	ATGAGGGTGGAAACTTGGAAAAG	NM_023456
POMC	TGGCCCTCCTGCTTCAGA	GGATGCAAGCCAGCAGGTT	NM_008895
SF-1	CCAGACCTTTATCTCCATTGTCG	AGTGTCATCTGGTCAGCCACCT	NM_139051.3
TRH	ACCTTGGTGCTGCCTTAGATTC	ATCTCCCCTCTCTTCGGCTTC	NM_009426.2

Abbreviations: HPRT1, hypoxanthine guanine phosphoribosyl transferase 1; Leptin R, leptin receptor; SF-1, steroidogenic factor 1.

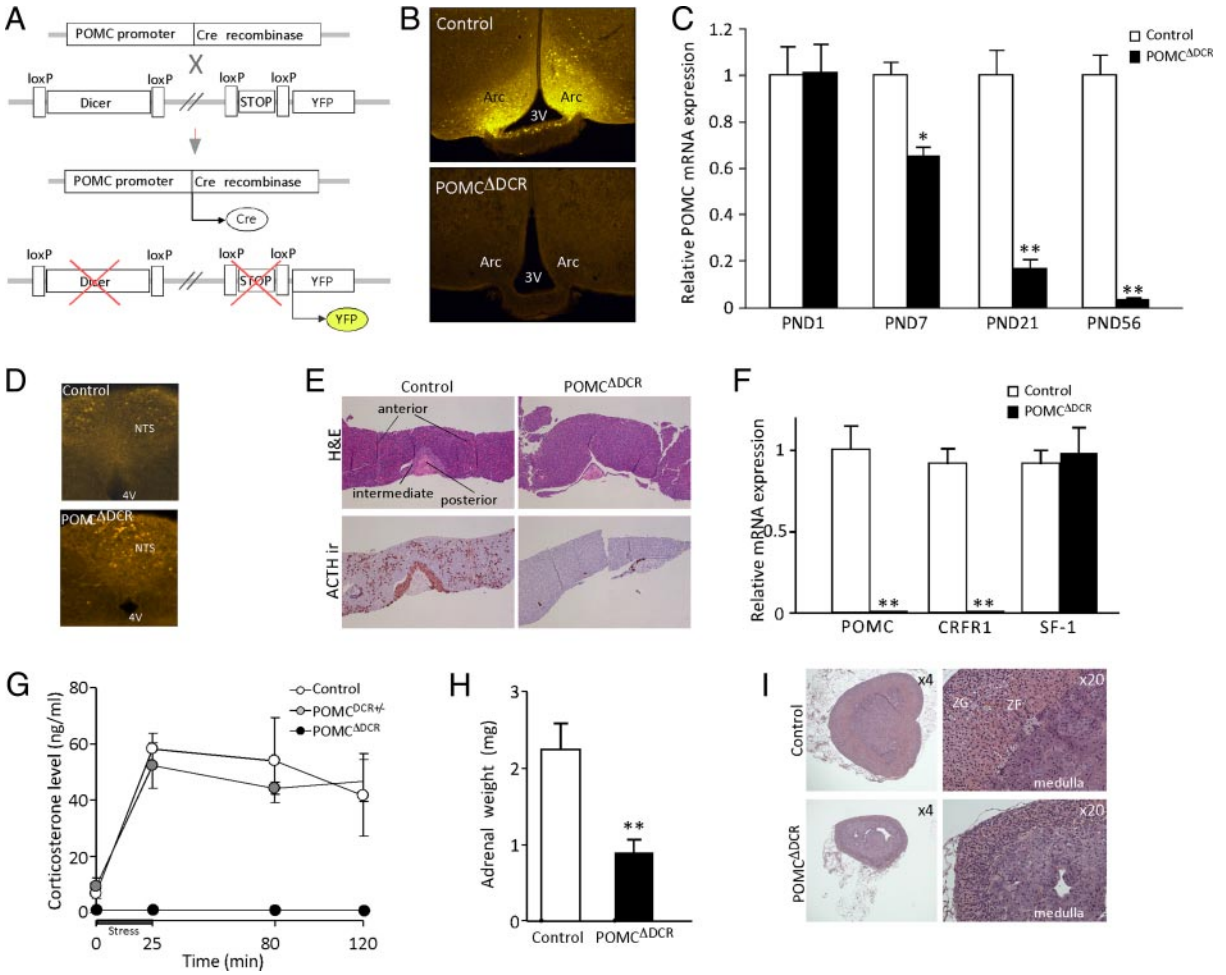

Figure 1. Establishment and verification of POMC$^{\Delta DCR}$ genetic mouse model. A, Schematic representation of Dicer deletion specifically in POMC-expressing cells. A mouse line expressing Cre recombinase specifically in POMC-expressing cells were cross-bred with mice carrying both floxed-dicer and floxed-transcriptional stop-YFP alleles. POMC cells undergo Cre-mediated recombination of loxP sites, leading to the ablation of the *Dicer* gene and the induction of YFP expression. B, Representative immunofluorescence of Cre-induced YFP expression in the arcuate nucleus of POMC$^{\Delta DCR}$ and control littermates, indicative of the loss of POMC neurons in POMC$^{\Delta DCR}$ mice. C, Hypothalamic relative POMC expression level at different postnatal days shows the kinetics of POMC neuronal loss (n = 4–6). D, Immunofluorescence of Cre-induced YFP expression in the hindbrain of POMC$^{\Delta DCR}$ and control littermates, indicative of intact POMC neurons in POMC$^{\Delta DCR}$ mice. E, ACTH and H&E staining of pituitaries obtained from POMC$^{\Delta DCR}$ and control littermates demonstrate loss of POMC-expressing cells in pituitary anterior and intermediate lobes. F, Pituitary relative POMC and CRFR1 mRNA expression is in line with the loss of pituitary corticotropes (n = 5–6). G, Basal and stress-induced corticosterone levels showing blunted response in POMC$^{\Delta DCR}$ mice (n = 5–7). H, Adrenal weight of POMC$^{\Delta DCR}$ and control littermates. I, H&E staining of adrenals obtained from POMC$^{\Delta DCR}$ and control littermates demonstrate the reduced adrenal size and the atrophy of the zona fasciculata layer. *, $P < .05$; **, $P < .01$ vs control. Values are expressed as the mean ± SEM. ir, immunoreactivity; ZF, zona faciculata; ZG, zona glomerulosa.

83% in POMC-mRNA expression levels, respectively (Figure 1C). POMC-mRNA expression was similar in mice heterozygous for the *Dicer* allele (POMC$^{DCR+/-}$) and control mice in all the tested time points (data not shown), indicating that loss of only 1 dicer allele does not lead to POMC neuronal loss. In contrast to the hypothalamus, POMC expression in the NTS was not affected, as demonstrated by immunostaining for YFP (Figure 1D).

Loss of POMC-expressing cells was evident in the pituitaries of POMC$^{\Delta DCR}$ mice. ACTH immunostaining was negative in both the anterior and the intermediate lobes of the pituitary gland (Figure 1E). Furthermore, there was marked atrophy of the pituitary intermediate lobe, indicating loss of melanotrope cells, which are the predominant cell type in this region (Figure 1E). POMC and corticotropin-releasing factor receptor 1 (CRFR1) mRNA were undetectable in the pituitary gland of POMC$^{\Delta DCR}$, consistent with loss of corticotropes (Figure 1F). In contrast, steroidogenic factor 1, a gonadotrope marker, was expressed at similar levels in POMC$^{\Delta DCR}$ and control animals. As expected from the loss of the entire population of pituitary corticotrope cells, both basal and stress-induced corticosterone levels were undetectable in these mice (Figure 1G). Loss of ACTH tone led

to changes in both adrenal weight and morphology. Adrenal weight of POMC$^{\Delta DCR}$ mice was markedly reduced compared with that of control animals (Figure 1H), which could be mainly attributed to atrophy of the zona fasciculata layer (Figure 1I).

POMC$^{\Delta DCR}$ mice develop obesity and diabetes at an early age

At 4 weeks of age, it was already evident that both male and female POMC$^{\Delta DCR}$ mice were heavier than POMC$^{DCR+/-}$ and control littermates (males, 19.28 ± 0.75, 17.07 ± 0.57, and 14.2 ± 0.96 g, respectively, $P < .001$; females, 19.35 ± 0.62, 14.58 ± 0.32, and 14.6 ± 0.91 g, respectively, $P < .001$; Figure 2, A and B). Although at this age it was apparent that POMC$^{DCR+/-}$ males' weight was higher than control mice ($P < .05$), this difference was subsequently lost as POMC$^{\Delta DCR}$ weight curves rapidly diverged upward in comparison with POMC$^{DCR+/-}$ and control curves that progressed in parallel (2 way ANOVA $P < .0001$ for both genders, Figure 2, A and B). We next explored the possibility that POMC$^{DCR+/-}$ may have an intermediate obese phenotype when challenged with a high-fat diet, as has been described in heterozygous *pomc* mice (8). Weight gain was similar to that observed in controls (data not shown), reflecting the similar hypothalamic POMC-mRNA levels found in these genotypes. In addition to the prominent weight gain, the POMC$^{\Delta DCR}$ mice showed a significant increase in percentage fat mass and a decrease in lean mass compared with control or POMC$^{DCR+/-}$ littermates (Figure 2C). Interestingly, despite the higher percentage of fat mass, total cholesterol, high-density lipoprotein cholesterol, and low-density lipoprotein cholesterol were significantly lower in POMC$^{\Delta DCR}$ mice, whereas triglyceride levels were similar (Figure 2, D–G). Fasting glucose levels were dramatically elevated in POMC$^{\Delta DCR}$ mice (141.5 ± 5.0 vs 94.3 ± 13.2 in control mice, $P < .05$) and a glucose tolerance test revealed marked glucose intolerance in POMC$^{\Delta DCR}$ mice (ANOVA $P < .01$), with peak glucose levels reaching 357 ± 34 mg/dL vs 247 ± 13 mg/dL at 30 minutes ($P < .001$) (Figure 2H).

Insulin levels and HOMA-IR were already significantly higher in POMC$^{\Delta DCR}$ mice at the age of 7 weeks (Table 2). Interestingly, at 7 weeks of age, basal GLP-1 levels were slightly higher in the POMC$^{\Delta DCR}$ mice (93 ± 1.4 pg/mL) in comparison with control mice (85 ± 0.7 pg/mL, $P = .005$), but at 4 months, this difference was lost (Table 2).

Food intake and metabolic rate are altered in POMC$^{\Delta DCR}$ mice

At the age of 6 weeks, food intake was significantly higher in POMC$^{\Delta DCR}$ mice (Figure 3A), but when corrected to metabolic body weight (BW$^{\hat{}0.75}$), the food intake was significantly lower (Figure 3B). In adulthood, a nonsignificant tendency toward lower absolute food intake of the POMC$^{\Delta DCR}$ mice was observed (Figure 3A). However, when corrected to metabolic body weight, the food intake was significantly lower relative to control littermates (Figure 3, A and B).

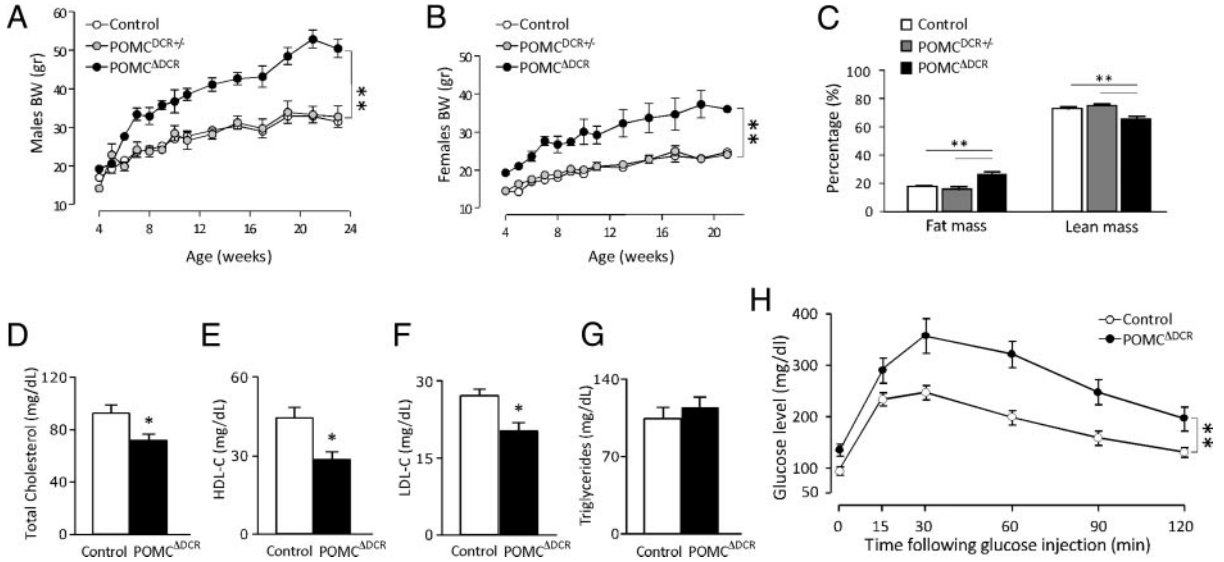

Figure 2. Increased body weight and adiposity in POMC$^{\Delta DCR}$ mice is accompanied by alterations in lipids and glucose homeostasis. A and B, Growth curves of males (A) and females (B) POMC$^{\Delta DCR}$, POMC$^{DCR+/-}$, and control littermates (n = 7–12), demonstrating a significant increase in body weight in the POMC$^{\Delta DCR}$ mice. C, Body composition demonstrating increased adiposity and reduced lean mass in POMC$^{\Delta DCR}$ mice (n = 7). D–G, Total cholesterol (D), high-density lipoprotein (HDL) cholesterol (E), low-density lipoprotein (LDL) cholesterol (F), and triglycerides (G), demonstrating altered lipid profile of POMC$^{\Delta DCR}$ mice. H, Glucose tolerance test showing impaired glucose tolerance in POMC$^{\Delta DCR}$ mice (n = 6). *, $P < .05$; **, $P < .01$. Values are expressed as the mean ± SEM.

Table 2. Cytokine and HOMA-IR in Control and POMC$^{\Delta DCR}$ Mice

	Seven Weeks		Four Months	
	Control	POMC$^{\Delta DCR}$	Control	POMC$^{\Delta DCR}$
Insulin, ng/mL	1.12 ± 0.18	2.68 ± 0.63[a]	0.94 ± 0.21	1.99 ± 0.42[a]
HOMA-IR	11.98 ± 1.99	35.73 ± 9.78[a]	8.64 ± 2.31	23.22 ± 9.78[a]
Leptin, ng/mL	1.42 ± 0.21	6.60 ± 1.86[a]	2.34 ± 0.94	12.12 ± 2.87[b]
GLP-1, pg/mL	84.95 ± 0.75	93.06 ± 1.43[b]	84.62 ± 0.99	81.99 ± 1.66

[a] $P < .05$ compared with control mice at the same age.
[b] $P < .01$ compared with control mice at the same age.

Microstructural analysis of eating behavior was performed for the dark (active) phase of the day cycle. As seen in Table 3, the number of meals consumed as well as the food and water amount per meal was similar between the groups. Interestingly, POMC$^{\Delta DCR}$ mice meal duration was significantly longer due to slower eating rate.

Indirect calorimetry revealed that POMC$^{\Delta DCR}$ mice had a decreased metabolic rate, which was reflected by the reduction of both light and dark phase oxygen consumption and carbon dioxide production as well as decreased heat production (Figure 3, C–E). These changes were not reflected in the respiratory exchange ratio, which remained similar in both groups (not shown). The decrease in metabolic rate and energy expenditure could not be attributed to alteration in locomotor activity that was similar in both groups (Figure 3F).

POMC$^{\Delta DCR}$ mice had reduced body core temperature (Figure 4A) and reduced expression of UCP1, peroxisome proliferator-activated receptor γ coactivator 1α, β-3 adrenergic receptor (*Adrb3*), and type II iodothyronine deiodinase (*DIO2*), genes associated with thermogenesis in BAT (Figure 4, B and C), suggesting that the reduced heat production in these mice is a consequence of reduced sympathetic tone. The reduced expression of DIO2 as well as the reduced metabolic rate were not secondary to decreased thyroid function because free T_4 levels was similar in POMC$^{\Delta DCR}$ and control mice (Figure 4D). However, despite the equivalent free T_4 levels, hypothalamic TRH mRNA levels were significantly lower in POMC$^{\Delta DCR}$ mice (Figure 4E), probably reflecting the low melanocortinergic tone in these mice. To explore additional mechanistic changes that may contribute to the metabolic phenotype of POMC$^{\Delta DCR}$ mice, we have examined the hypothalamic mRNA expression levels of neuropeptides and receptors involved in the regulation of energy homeostasis as well as plasma levels of leptin. AgRP mRNA levels were robustly reduced by 87% ($P < .01$) in POMC$^{\Delta DCR}$ mice, potentially explaining the decreased food intake in these mice (Figure 4E). In accordance to the leptin resistance state associated with obesity, plasma leptin levels were already significantly elevated in 7-week-old POMC$^{\Delta DCR}$ mice, and a further increase was observed at the age of 4 months compared with the control mice (Table 2). The expression of hypothalamic leptin receptor, ghrelin receptor, and MC4Rs were decreased in the POMC$^{\Delta DCR}$ mice, whereas MC3R and NPY expression was similar to that found in the control mice (Figure 4E).

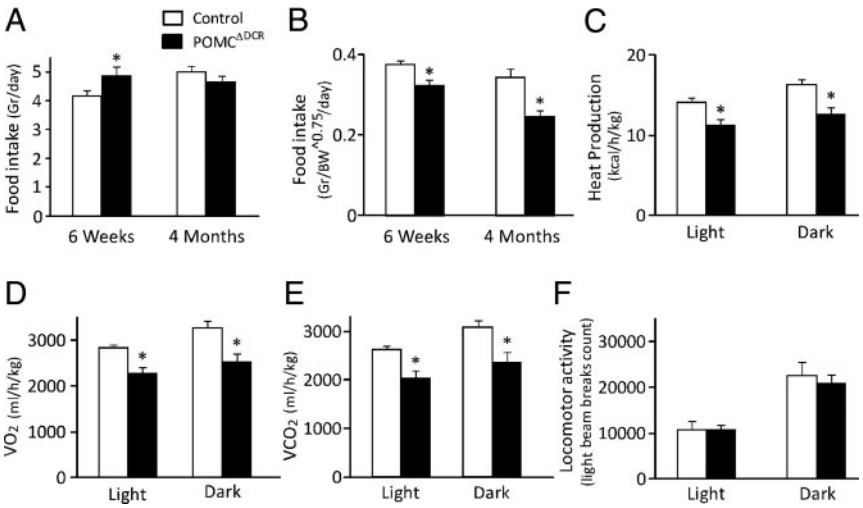

Figure 3. Food intake and metabolic rate are altered in POMC$^{\Delta DCR}$ mice. A and B, Daily food intake in young and adult POMC$^{\Delta DCR}$ and control littermates in absolute values (A) and normalized to metabolic body weight (BW$^{0.75}$) (B) demonstrated a significant decrease in food intake in the POMC$^{\Delta DCR}$ mice. C–E, Heat production (C), oxygen consumption (VO_2) (D), and carbon dioxide production (VCO_2) (E) are lower in adult POMC$^{\Delta DCR}$ mice during both the dark and light phases of the day cycle, indicative of lower metabolic rate. F, Locomotor activity is similar among experimental groups. Values are expressed as the mean ± SEM, *, $P < .05$; **, $P < .01$ vs control (n = 7–8).

POMC neuron ablation induced a basal state of enhanced anxiety

Because loss of corticotropes in POMC$^{\Delta DCR}$ mice resulted in inactivation of the hypothalamus-pituitary-adrenal (HPA) axis, we explored whether this affected the mice performance in anxiety-like be-

Table 3. Meal Structure Analysis of Control and POMC$^{\Delta DCR}$ Mice

	Control	POMC$^{\Delta DCR}$
Number of meals	11.1 ± 0.9	10.3 ± 0.4
Duration, min	10.1 ± 1.0	14.3 ± 1.2[a]
Food amount, g	0.28 ± 0.02	0.30 ± 0.02
Water amount, mL	0.16 ± 0.01	0.16 ± 0.01
Food to water ratio, g/mL	0.66 ± 0.14	0.65 ± 0.17
Eating rate, g/min	0.042 ± 0.004	0.027 ± 0.004[a]
Intermeal interval, min	58.6 ± 7.2	57.6 ± 3.2
Satiety, min/g	321.4 ± 37.1	347.8 ± 75.4

[a] $P < .05$ compared with control mice.

havioral tests. POMC$^{\Delta DCR}$ mice exhibit a robust anxiogenic phenotype as assessed by the dark-light transfer test, the elevated plus maze, and the acoustic startle response. In the dark-light transfer test, POMC$^{\Delta DCR}$ mice spent less time in the light compartment (Figure 5A), showed longer latency to enter the light compartment (Figure 5B), and traveled a shorter distance during the test (Figure 5C). In the elevated plus maze, the POMC$^{\Delta DCR}$ mice spent less time in the open arms (Figure 5D). The acoustic startle response test is known to be corticosterone independent because it is not modified by adrenalectomy (22). Therefore, we performed this test with the intent of analyzing the anxiety response while accounting for the absent stress induced corticosterone response in the POMC$^{\Delta DCR}$ mice. The POMC$^{\Delta DCR}$ and the control mice had similar reaction times (POMC$^{\Delta DCR}$: 9.64 ± 0.72 seconds; control: 8.46 ± 0.37 seconds), but the maximum response (Figure 5E) and the within-session rate of habituation (Figure 5F) were markedly higher and lower, respectively, in the POMC$^{\Delta DCR}$ mice. The anxiogenic phenotype of POMC$^{\Delta DCR}$ mice was accompanied by elevated levels of both corticotropin-releasing factor (CRF) and arginine-vasopressin (AVP), both known to have an anxiogenic effect (Figure 5G), and probably reflecting a compensatory response to the decreased POMC levels and to the absence of the negative feedback provided by corticosterone.

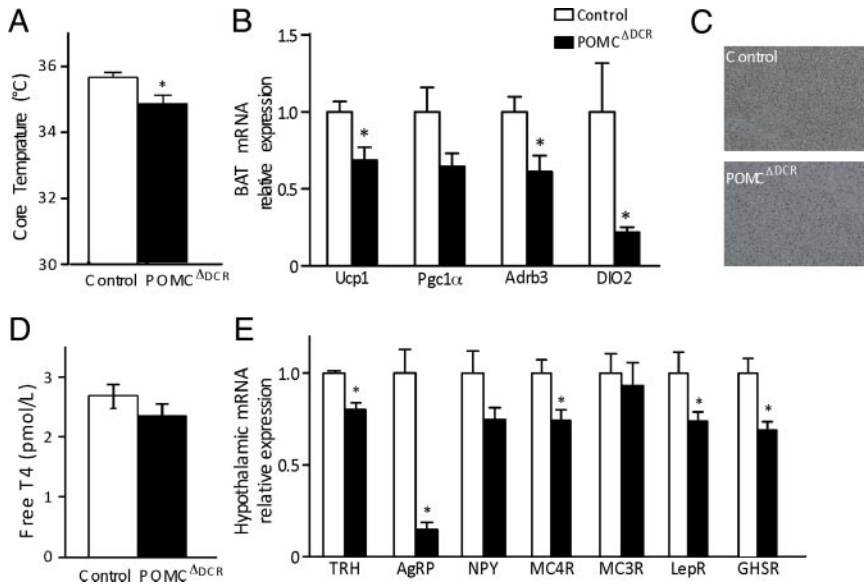

Figure 4. Reduced sympathetic tone and modified hypothalamic gene expression profile in POMC$^{\Delta DCR}$ mice. A, Core body temperature of POMC$^{\Delta DCR}$ and control mice. B, Gene expression profile of proteins associated with thermogenesis in BAT. C, Immunohistochemical staining of Ucp1 in BAT of POMC$^{\Delta DCR}$ and control littermates. D, Free T_4 levels demonstrate unaltered thyroid function in POMC$^{\Delta DCR}$ mice. E, Hypothalamic gene expression profile of peptides and receptors known to be involved in the regulation of energy homeostasis. Values are expressed as the mean ± SEM. *, $P < .05$ vs control (n = 5–7). LepR, leptin receptor.

Discussion

By deleting the ribonuclease III ribonuclease Dicer-1 gene specifically from POMC neurons and corticotropes, we succeeded in establishing a mouse model in which the POMC cells are ablated postnatally and mice are born with hypothalamic POMC-mRNA levels equivalent to that of the control littermates. By avoiding the partial embryonic lethality observed in previous models (8, 9) and by delaying POMC neuron ablation to the postnatal period, we may have reduced possible compensatory mechanisms that could confound the phenotype of these mice.

One of the main findings of the current study is that the obese phenotype generated by POMC neuron ablation is maintained by a decrease in energy expenditure without the expected increase in food intake, which one would anticipate from loss of the melanocortinergic tone. In fact, corrected food intake was decreased in young animals and even more so in adult POMC$^{\Delta DCR}$ mice, in striking contrast to the hyperphagia described in mice models of *pomc* gene deletion (8, 9, 23). One could speculate that ablation of POMC neurons abrogated feeding regulatory pathways that are not mediated through activation of the *pomc* gene. Possible explanations for the decrease in food intake are the significantly reduced hypothalamic mRNA levels of the orexigenic peptide AgRP as well as that of the ghrelin receptor (GHSR). Reduced AgRP expression has also been described in the *pomc*-null mouse model generated by the group of O'Rahilly and colleagues (8, 24).

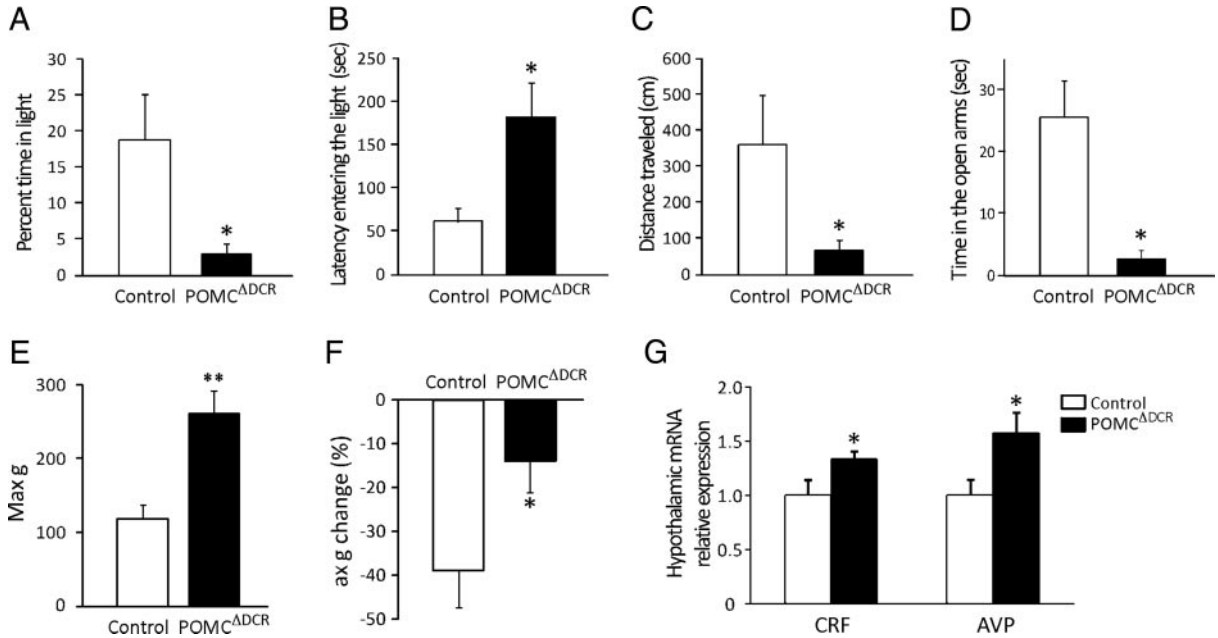

Figure 5. Ablation of POMC-expressing cells leads to increased anxiety-like behavior. A–D, Anxiety-like behaviors of POMC$^{\Delta DCR}$ and control littermates as measured by the dark-light transfer (DLT) (A–C) and by the elevated plus maze (EPM) tests (D). The reduced percentage of time spent in the light compartment (A), longer latency entering the light compartment (B), shorter distance traveled in the light compartment of the DLT (C), and the reduced time spent in the open arms of the EPM (D) are indicative of anxiogenic behavior. E and F, Anxiety-like behaviors as measured by the ASR. The increased maximal ASR (E) and reduced within-session ASR rate of habituation (F) points toward an increase in anxiety-like behavior. Hypothalamic expression of the anxiogenic peptides, CRF and AVP (G). *, $P < .05$; **, $P < .01$ vs control. Values are expressed as the mean ± SEM (n = 8–10). Max g, maximum response.

The absence of peripheral glucocorticoids is probably one of the major factors contributing to the reduced expression of AgRP because it has been shown that AgRP expression was dramatically reduced in adrenalectomized mice (25) and that corticosterone administration increased AgRP expression levels both on wild-type and *pomc*-null background (24, 25). The reduced expression of GHSR may also be partially attributed to the absence of glucocorticoids because dexamethasone was shown to stimulate the GHSR mRNA and protein expression in a hypothalamic cell line (26). The critical role played by glucocorticoids is well exemplified by the reversal of the obese phenotype and the restoration of the hypothalamic melanocortic tone in leptin-deficient ob/ob mice by adrenalectomy (25).

Of note, in the *pomc*-null mice characterized by Smart et al (23), a similar tendency for a decrease in food intake toward adulthood was found; although corrected food intake was higher than controls at 6 weeks, it was significantly lower at 26 weeks (23). A similar transient hyperphagia has been described in mice lacking leptin receptors from both POMC and AgRP neurons (27), suggesting a differential weight regulation at young age. A parallel could be made to humans harboring heterozygous mutations in the MC4R, who present with increased appetite in childhood, with the progressive amelioration of the phenotype such that the ad libitum energy intake at the age group of 11–15 years was approximately half of that in children up to 5 years of age, as expressed by kilocalories per kilogram of lean mass (28).

Two significantly different paradigms have been previously used to study the effects of acute or gradual POMC neuron ablation on parameters of energy homeostasis. Diphtheria toxin administration to adult mice selectively expressing a diphtheria toxin receptor in POMC neurons caused acute degeneration or necrosis of more than 85% of these neurons within 72 hours of treatment initiation (29). An increase in food intake and body weight, without changes in blood glucose levels, was observed during the 10-day follow-up period. In the second model, POMC-expressing cells were gradually ablated by selective deletion of the mitochondrial transcription factor A (*tfam*), leading to a progressive loss of cellular respiration and consequent cell death (30). Reduction in α-MSH immunostaining was evident in *pomc*-specific *tfam* mutant mice only at 7 months of age, although excess weight gain, secondary to both increased food intake and reduced energy expenditure, was already apparent at 4 months of age and proceeded progressively compared with control animals and as such were suggested as a model for age-related obesity. Clearly, other than the resultant obese phenotype, it is extremely difficult to draw

other parallels between our model, in which POMC-cell ablation is generated in the neonatal period, and those in which neuronal loss occurs acutely at adulthood or gradually toward senescence.

Another major point to be taken from our study is that the main factor leading to the maintenance of obesity in adulthood was the decreased metabolic rate and not increased food consumption. The decreased metabolic rate of $POMC^{\Delta DCR}$ mice could be explained by alteration in BAT activity. Energy expenditure in BAT is highly regulated by sympathetic stimulation. Norepinephrine released from sympathetic nerve terminals activates the BAT via binding to β-adrenergic receptors. Adrenergic innervations regulate both Ucp1 expression and activity and increases DIO2 activity, leading to increased intracellular concentrations of T_3 (31). The reduced BAT Adrb3 expression in $POMC^{\Delta DCR}$ mice suggests a reduction in sympathetic tone and may explain, at least in part, the reduction in Ucp1 and DIO2 expression level. Because NTS POMC neurons are intact in $POMC^{\Delta DCR}$ mice, the reduced sympathetic tone could be due to changes in sympathetic activation arising from the hypothalamus. This can involve both first-order neurons because POMC neurons were demonstrated, using retrograde tracing to project polysynaptically to BAT (32) or via second-order neurons in the PVN, a key source of autonomic outflow (33).

Maintenance of obesity due to diminished metabolic rate cannot be overemphasized in view of its clinical implications for the care of patients suffering from hypothalamic obesity. These subjects, frequently children, develop obesity secondary to hypothalamic damage by tumors such as craniopharyngiomas or secondary to their treatment (34). In general, parents or family members report an acute increase in food intake at diagnosis or shortly after surgical tumor excision, although, to the best of our knowledge, this hyperphagia has not been formally quantified. Nevertheless, at a later stage of the disease, these patients were found to have normal or even decreased food intake, coupled with a significant reduction in basal metabolic rate (35, 36), which may be attributed to the abnormal sympathetic tone secondary to hypothalamic damage. Hence, clinical interventions based on calorie restriction are doomed to fail in achieving sustained weight loss, thus leading to frustration and further psychological distress (34). Interestingly, obese subjects heterozygous for *mc4r* were shown to have decreased urinary norepinephrine excretion (37), and their body mass index was inversely correlated with vasoconstrictive muscle sympathetic nerve activity, a direct measure of central sympathetic nervous outflow (38). Thus, in addition to their reported hyperphagia, reduced metabolic rate emerges as another important factor to be addressed in patients harboring *mc4r* mutations, which accounts for approximately 5% of cases with body mass index greater than 30 kg/m^2 (28).

The phenotypic characterization of our model highlighted another significant difference consequent of POMC neuron ablation compared with knockout of the *pomc* gene: $POMC^{\Delta DCR}$ mice were diabetic and insulin resistant from an early age, in contrast to the model created by Hochgeschwender and colleagues (9, 39) in which mice with a deletion of the coding region for all POMC peptides had normal fasting and insulin levels as well as normal glucose tolerance, despite their marked obesity. In the mouse model generated by the group of O'Rahilly and colleagues (8, 24), POMC-deficient mice have higher fed blood glucose but equivalent insulin levels compared with their wild-type littermates and become diabetic only upon corticosterone administration from weaning but not in adulthood. Similarly, normoinsulinemic POMC-null mice developed insulin resistance only upon restoration of HPA axis function by introducing a POMC transgene selectively in the pituitary gland.

Our results confirm and strengthen the published data indicating the central role of POMC neurons in the regulation of whole-body glucose homeostasis, including glucose sensing (40) and modulation of pancreatic glucagon secretion and hepatic insulin sensitivity (41). Activation of leptin, insulin (42), and serotonin 2C receptors (43) on POMC neurons has been shown to regulate different aspects of glucose homeostasis. The observation that isolated *pomc* gene ablation causes no or minimal alteration in glucose levels may suggest that the melanocortinergic pathways may not be involved or essential in mediating these effects. Alternatively, it is possible that *pomc* gene-deleted mice developed in utero compensatory mechanisms to circumvent the striking disruption of glucose homeostasis that was observed with POMC neuron ablation.

In view of the expanding interest in the relationship between stress-regulatory systems and eating behavior, we explored the effect of POMC neuron ablation on anxiety parameters. We hypothesized that $POMC^{\Delta DCR}$ mice would exhibit decreased anxiety behavior in view of the known anxiogenic effects of α-MSH through the activation of MC4R (44). Surprisingly, $POMC^{\Delta DCR}$ mice exhibit a robust anxiogenic phenotype as assessed by several well-established behavioral tests for assessing anxiety-like behavior. The elevated CRF and AVP levels, both anxiogenic peptides, may reflect a compensatory response to the decreased POMC levels and to the absence of the negative feedback provided by corticosterone (44). Additional detailed pharmacological or genetic studies are needed to fully elucidate the molecular and cellular

mechanisms that are mediating the behavioral changes observed in these mice. In this sense, this is a unique model to study the specific effects of CRF on anxiety, independent of the effects secondary to the increased HPA axis activation characteristic of models of CRF overexpression or central CRF administration (45). The observed decrease in ghrelin receptors, possibly leading to reduced ghrelin action may be an additional contributory factor because this peptide has been shown to have anxiolytic and antidepressant effects (46, 47).

In summary, this model emphasizes that the main mechanism leading to obesity secondary to POMC neuron ablation is a reduction in metabolic rate and not appetite control dysregulation. Furthermore, unlike isolated deletion of the *pomc* gene, loss of POMC neurons leads to pronounced insulin resistance and diabetes. Finally, the increased anxiety exhibited by these mice possibly indicates that up-regulation of CRF and/or AVP tone mediate the stress response despite the loss of melacortinergic tone and the lack of HPA axis activation.

Acknowledgments

We thank Mr S. Ovadia for his devoted assistance with animal care. We also thank Dr R. Eilam for her assistance with the BAT immunostaining.

Address all correspondence and requests for reprints to: Alon Chen, PhD, Department of Neurobiology, Weizmann Institute of Science, Rehovot, Israel 76100. E-mail: alon.chen@weizmann.ac.il; or Yael Kuperman, PhD, Department of Veterinary Resources, Weizmann Institute of Science, Rehovot, Israel 76100, E-mail: yael.kuperman@weizmann.ac.il.

This work was supported by FP7 Grant 260463 from the European Research Council; a research grant from the Israel Science Foundation; a research grant from Roberto and Renata Ruhman; a research grant from the Legacy Heritage Biomedical Science Partnership; a grant from Mr and Mrs Mike Kahn; a research grant from Mr Jorge David Ashkenazi; a research grant from Mr and Mrs Barry Wolfe; and a research grant from Nella and Leon Benoziyo Center for Neurosciences.

Disclosure Summary: The authors have nothing to disclose.

References

1. **Yach D, Stuckler D, Brownell KD.** Epidemiologic and economic consequences of the global epidemics of obesity and diabetes. *Nat Med*. 2006;12:62–66.
2. **Horvath TL.** The hardship of obesity: a soft-wired hypothalamus. *Nat Neurosci*. 2005;8:561–565.
3. **Woods SC, D'Alessio DA.** Central control of body weight and appetite. *J Clin Endocrinol Metab*. 2008;93:S37–S50.
4. **Balthasar N.** Feeding signals to the hungry mind. *Exp Physiol*. 2009;94:857–866.
5. **Krude H, Biebermann H, Luck W, Horn R, Brabant G, Gruters A.** Severe early-onset obesity, adrenal insufficiency and red hair pigmentation caused by POMC mutations in humans. *Nat Genet*. 1998;19:155–157.
6. **Jackson RS, Creemers JW, Ohagi S, et al.** Obesity and impaired prohormone processing associated with mutations in the human prohormone convertase 1 gene. *Nat Genet*. 1997;16:303–306.
7. **Farooqi IS, Yeo GS, Keogh JM, et al.** Dominant and recessive inheritance of morbid obesity associated with melanocortin 4 receptor deficiency. *J Clin Invest*. 2000;106:271–279.
8. **Challis BG, Coll AP, Yeo GS, et al.** Mice lacking pro-opiomelanocortin are sensitive to high-fat feeding but respond normally to the acute anorectic effects of peptide-YY(3–36). *Proc Natl Acad Sci USA*. 2004;101:4695–4700.
9. **Yaswen L, Diehl N, Brennan MB, Hochgeschwender U.** Obesity in the mouse model of pro-opiomelanocortin deficiency responds to peripheral melanocortin. *Nat Med*. 1999;5:1066–1070.
10. **Gingrich JA, Hen R.** The broken mouse: the role of development, plasticity and environment in the interpretation of phenotypic changes in knockout mice. *Curr Opin Neurobiol*. 2000;10:146–152.
11. **Konopka W, Kiryk A, Novak M, et al.** MicroRNA loss enhances learning and memory in mice. *J Neurosci*. 2010;30:14835–14842.
12. **Srinivas S, Watanabe T, William CM, et al.** Cre reporter strains produced by targeted insertion of EYFP and ECFP into the ROSA26 locus. *BMC Dev Biol*. 2001;1:4.
13. **Harfe BD, McManus MT, Mansfield JH, Hornstein E, Tabin CJ.** The RNaseIII enzyme Dicer is required for morphogenesis but not patterning of the vertebrate limb. *Proc Natl Acad Sci USA*. 2005;102:10898–10903.
14. **Ezzat S, Mader R, Yu S, Ning T, Poussier P, Asa SL.** Ikaros integrates endocrine and immune system development. *J Clin Invest*. 2005;115:1021–1029.
15. **Matthews DR, Hosker JP, Rudenski AS, Naylor BA, Treacher DF, Turner RC.** Homeostasis model assessment: insulin resistance and β-cell function from fasting plasma glucose and insulin concentrations in man. *Diabetologia*. 1985;28:412–419.
16. **Rabiner LR.** A tutorial on hidden Markov models and selected applications in speech recognition. *Proc IEEE*. 1989;77:257–286.
17. **Baum LE, Petrie T, Soules G, Weiss N.** A maximization technique occurring in the statistical analysis of probabilistic functions of Markov chains. *Ann Math Statist*. 1970;41:164–171.
18. **Viterbi A.** Error bounds for convolutional codes and an asymptotically optimum decoding algorithm. *IEEE Trans Inf Theory*. 1967;13:260–269.
19. **Neufeld-Cohen A, Tsoory MM, Evans AK, et al.** A triple urocortin knockout mouse model reveals an essential role for urocortins in stress recovery. *Proc Natl Acad Sci USA*. 2010;107:19020–19025.
20. **Lin J, Wu PH, Tarr PT, et al.** Defects in adaptive energy metabolism with CNS-linked hyperactivity in PGC-1α null mice. *Cell*. 2004;119:121–135.
21. **Balthasar N, Coppari R, McMinn J, et al.** Leptin receptor signaling in POMC neurons is required for normal body weight homeostasis. *Neuron*. 2004;42:983–991.
22. **Lee Y, Schulkin J, Davis M.** Effect of corticosterone on the enhancement of the acoustic startle reflex by corticotropin releasing factor (CRF). *Brain Res*. 1994;666:93–98.
23. **Smart JL, Tolle V, Low MJ.** Glucocorticoids exacerbate obesity and insulin resistance in neuron-specific proopiomelanocortin-deficient mice. *J Clin Invest*. 2006;116:495–505.
24. **Coll AP, Challis BG, Lopez M, Piper S, Yeo GS, O'Rahilly S.** Proopiomelanocortin-deficient mice are hypersensitive to the adverse metabolic effects of glucocorticoids. *Diabetes*. 2005;54:2269–2276.
25. **Makimura H, Mizuno TM, Roberts J, Silverstein J, Beasley J, Mobbs CV.** Adrenalectomy reverses obese phenotype and restores hypothalamic melanocortin tone in leptin-deficient ob/ob mice. *Diabetes*. 2000;49:1917–1923.

26. **Kageyama K, Akimoto K, Yamagata S, et al.** Dexamethasone stimulates the expression of ghrelin and its receptor in rat hypothalamic 4B cells. *Regul Pept*. 2012;174:12–17.
27. **van de Wall E, Leshan R, Xu AW, et al.** Collective and individual functions of leptin receptor modulated neurons controlling metabolism and ingestion. *Endocrinology*. 2008;149:1773–1785.
28. **Farooqi IS, Keogh JM, Yeo GS, Lank EJ, Cheetham T, O'Rahilly S.** Clinical spectrum of obesity and mutations in the melanocortin 4 receptor gene. *N Engl J Med*. 2003;348:1085–1095.
29. **Gropp E, Shanabrough M, Borok E, et al.** Agouti-related peptide-expressing neurons are mandatory for feeding. *Nat Neurosci*. 2005;8:1289–1291.
30. **Xu AW, Kaelin CB, Morton GJ, et al.** Effects of hypothalamic neurodegeneration on energy balance. *PLoS Biol*. 2005;3:e415.
31. **Lowell BB, Flier JS.** Brown adipose tissue, β3-adrenergic receptors, and obesity. *Annu Rev Med*. 1997;48:307–316.
32. **Oldfield BJ, Giles ME, Watson A, Anderson C, Colvill LM, McKinley MJ.** The neurochemical characterisation of hypothalamic pathways projecting polysynaptically to brown adipose tissue in the rat. *Neuroscience*. 2002;110:515–526.
33. **Kotz CM, Wang C, Levine AS, Billington CJ.** Urocortin in the hypothalamic PVN increases leptin and affects uncoupling proteins-1 and -3 in rats. *Am J Physiol Regul Integr Comp Physiol*. 2002;282:R546–R551.
34. **Lustig RH.** Hypothalamic obesity after craniopharyngioma: mechanisms, diagnosis, and treatment. *Front Endocrinol (Lausanne)*. 2011;2:60.
35. **Holmer H, Pozarek G, Wirfalt E, et al.** Reduced energy expenditure and impaired feeding-related signals but not high energy intake reinforces hypothalamic obesity in adults with childhood onset craniopharyngioma. *J Clin Endocrinol Metab*. 2010;95:5395–5402.
36. **Shaikh MG, Grundy RG, Kirk JM.** Reductions in basal metabolic rate and physical activity contribute to hypothalamic obesity. *J Clin Endocrinol Metab*. 2008;93:2588–2593.
37. **Greenfield JR, Miller JW, Keogh JM, et al.** Modulation of blood pressure by central melanocortinergic pathways. *N Engl J Med*. 2009;360:44–52.
38. **Sayk F, Heutling D, Dodt C, et al.** Sympathetic function in human carriers of melanocortin-4 receptor gene mutations. *J Clin Endocrinol Metab*. 2010;95:1998–2002.
39. **Hochgeschwender U, Costa JL, Reed P, Bui S, Brennan MB.** Altered glucose homeostasis in proopiomelanocortin-null mouse mutants lacking central and peripheral melanocortin. *Endocrinology*. 2003;144:5194–5202.
40. **Parton LE, Coppari R, Enriori PJ, et al.** Glucose sensing by POMC neurons regulates glucose homeostasis and is impaired in obesity. *Nature*. 2007;449:228–232.
41. **Berglund ED, Vianna CR, Donato J Jr, et al.** Direct leptin action on POMC neurons regulates glucose homeostasis and hepatic insulin sensitivity in mice. *J Clin Invest*. 2012;122:1000–1009.
42. **Hill JW, Elias CF, Fukuda M, et al.** Direct insulin and leptin action on pro-opiomelanocortin neurons is required for normal glucose homeostasis and fertility. *Cell Metab*. 2010;11:286–297.
43. **Xu Y, Berglund ED, Sohn JW, et al.** 5-HT2CRs expressed by pro-opiomelanocortin neurons regulate insulin sensitivity in liver. *Nat Neurosci*. 2010;13:1457–1459.
44. **Chaki S, Okuyama S.** Involvement of melanocortin-4 receptor in anxiety and depression. *Peptides*. 2005;26:1952–1964.
45. **Bale TL, Vale WW.** CRF and CRF receptors: role in stress responsivity and other behaviors. *Annu Rev Pharmacol Toxicol*. 2004;44:525–557.
46. **Lutter M, Sakata I, Osborne-Lawrence S, et al.** The orexigenic hormone ghrelin defends against depressive symptoms of chronic stress. *Nat Neurosci*. 2008;11:752–753.
47. **Zhou Z, Zhu G, Hariri AR, et al.** Genetic variation in human NPY expression affects stress response and emotion. *Nature*. 2008;452:997–1001.